# Quantum hydrodynamics of a polariton fluid: pure energy relaxation terms

D. A. Saltykova,[1] A. V. Yulin,[1] and I. A. Shelykh[2]

[1]*ITMO University, St. Petersburg 197101, Russia*

[2]*Science Institute, University of Iceland, Dunhagi 3, IS-107 Reykjavik, Iceland*

(Dated: April 10, 2025)

Cavity polaritons, hybrid half-light half-matter excitations in quantum microcavities in the strong-coupling regime demonstrate clear signatures of quantum collective behavior, such as analogues of BEC and superfluidity at surprisingly high temperatures. The analysis of the formation of these states demands an account of the relaxation processes in the system. Although there are well-established approaches for the description of some of them, such as finite lifetime polariton, an external optical pump, and coupling with an incoherent excitonic reservoir, the treatment of pure energy relaxation in a polariton fluid still remains a puzzle. Here, based on the quantum hydrodynamics approach, we derive the corresponding equations where the energy relaxation term appears naturally. We analyze in detail how it affects the dynamics of polariton droplets and the dispersion of elementary excitations of a uniform polariton condensate. Although we focus on the case of cavity polaritons, our approach can be applied to other cases of bosonic condensates, where the processes of energy relaxation play an important role.

The physics of quantum fluids represents a major part of modern condensed matter and atomic physics. In the low-temperature limit the ensembles of identical quantum particles can form macroscopically coherent states corresponding to Bose-Einstein condensates (BECs) and demonstrate the remarkable property of superfluidity. This phenomenon is well studied in the domain of cold atomic gases, where the dynamics of condensate droplets can be modeled by the Gross-Pitaevskii equation for the macroscopic wavefunction (order parameter) of the condensate [1]:

$$i\hbar \frac{\partial \psi}{\partial t} = -\frac{\hbar^2}{2m}\nabla^2\psi + U\psi + g|\psi|^2\psi. \qquad (1)$$

The first term on the right-hand side corresponds to a kinetic energy of the condensed particles, the second term describes an interaction with an external potential corresponding to an optical or magnetic trap, and the last non-linear term corresponds to interatomic interactions treated within the framework of the mean-field and s-wave scattering approximations. Gross-Pitaevskii equation gives a perfect description of the evolution of a conservative system with both the number of particles $N = \int |\psi(\mathbf{r}, t)|^2 d^2\mathbf{r}$ and the total energy:

$$H = \int \left[ \frac{\hbar^2}{2m}|\nabla\psi|^2 + U|\psi|^2 + \frac{g}{2}|\psi|^4 \right] d^2\mathbf{r}. \qquad (2)$$

The characteristic temperatures of the BEC phase transition for cold atomic gases lie in the nanokelvin diapason, which is related to the large mass of condensing atoms, such as isotopes of sodium and rubidium. This motivated the search of analogues of BECs in condensed matter systems, where effective masses of various bosonic quasiparticles are several orders of magnitude smaller, and one can expect formation of quantum collective states at much higher temperatures.

One of the attractive possibilities is the use of ensembles of exciton polaritons (also known as cavity polaritons), which appear when a strong coupling regime between excitonic and photonic modes is realized in an optical microresonator [2, 3]. Being composite half-light-half-matter particles, polaritons inherit an extremely small effective mass (about $10^{-5}$ of the mass of free electrons) and large coherence length (in the mm scale) [4] from their photonic component. However, the presence of an excitonic component results in efficient polariton-polariton interactions, which lead to an extremely strong nonlinear optical response. The polariton BEC and superfluidity were experimentally observed at surprisingly high temperatures under both optical [5–8] and electrical [9] excitation.

In addition to the difference in effective masses, there are several important distinctions between polaritonic and atomic systems.

First, polaritons can be directly created optically and have finite lifetimes because of the possibility for the photons to leave the system through the partially transparent Bragg mirrors.

Second, the presence of the excitonic fraction in a polariton makes possible efficient polariton-phonon interaction, which can both couple polaritons to an ensemble of incoherent excitons and lead to the energy relaxation within the polariton liquid itself.

These differences require substantial modifications of the dynamic equation 1. The finite lifetime of polaritons and an external coherent pump can also be introduced straightforwardly as a simple linear decay term and a complex time exponent source on the right-hand side of the equation 1 [10]. The incoherent pump and the coupling between polaritons and incoherent excitons are usually described in the framework of the Wouters-Carusotto model, which was first formulated for scaler polaritons [11] and then generalized for the spinor case [12].

Regarding the relaxation of energy within the condensate, there have been attempts, following the original approach of Pitaevskii [13], to include it in the phenomenological model by making the Hamiltonian non-Hermitian as $\hat{H} \to (1 - \Lambda)\hat{H}$, where $\Lambda$ is a small dimensionless parameter that controls the strength of dissipation [14]. However, it can be easily seen that this energy-dependent damping does not conserve the total number of particles in the condensate and therefore cannot be viewed as pure energy relaxation.

The present paper represents an attempt to construct the theory of pure energy relaxation in a polariton system. We base our consideration on the quantum hydrodynamics approach, describing the system dynamics via set of classical field Hamilton equations for canonically conjugated variables of concentration and phase two and introducing relaxation in a natural way by adding the gradient term. We analyze how this term affects the dynamics of the polariton droplets and dispersion of the elementary excitations. We consider the scalar case, focusing on pure energy relaxation only, leaving the spinor case and a description of polarization and spin relaxation for follow-up work.

Our goal here is not to present a modeling of system dynamics in any particular experimental configuration, but rather to focus on the fundamental role of the damping mechanisms, which were overlooked before. Therefore, for the reason of clarity of the presentation, in our analysis we neglect all other dissipative processes, such as finite lifetimes, external pumping, and coupling with an incoherent excitonic reservoir, for which well established theoretical approaches exist already. These terms can be easily taken into account when analyzing a particular set of experimental data.

*Dynamic equations.* Let us note that the conservative Gross-Pitaevskii equation 1 is nothing but an equation for a classical field, which can be obtained using the least action $\delta S = 0$, $S = \int \mathscr{L} d^2\mathbf{r} dt$ with the Lagrangian being (we take $U = 0$ and the spatial dimensionality two characteristic for polariton systems):

$$\mathscr{L} = \frac{i\hbar}{2}\left(\psi^*\frac{\partial\psi}{\partial t} - \psi\frac{\partial\psi^*}{\partial t}\right) - \frac{\hbar^2}{2m}(\nabla\psi^*)(\nabla\psi) - \frac{g}{2}\left(\psi^*\psi\right)^2. \tag{3}$$

Using the Madelung representation of a field function in terms of density-phase variables,

$$\psi = \sqrt{\rho}e^{-i\theta}, \tag{4}$$

one gets:

$$\mathscr{L} = \hbar\rho\partial_t\theta - \frac{\hbar^2}{2m}\left[(\nabla\sqrt{\rho})^2 + \rho(\nabla\theta)^2\right] - \frac{g}{2}\rho^2. \tag{5}$$

From this expression it follows that the angle $\theta$ can be considered as a generalized field coordinate, while the density $\rho$ corresponds to canonically conjugated momentum as:

$$\pi = \frac{\partial\mathscr{L}}{\partial(\partial_t\theta)} = \hbar\rho \tag{6}$$

with the canonical field Hamiltonian being

$$\mathscr{H} = \pi\partial_t\theta - \mathscr{L} = \frac{\hbar^2}{2m}\left[(\nabla\sqrt{\rho})^2 + \rho(\nabla\theta)^2\right] + \frac{g}{2}\rho^2. \tag{7}$$

The dynamic field equation can be thus represented in the Hamiltonian form as:

$$\partial_t\pi = \hbar\partial_t\rho = -\frac{\delta\mathscr{H}}{\delta\theta} = \frac{\hbar^2}{m}\nabla(\rho\nabla\theta), \tag{8}$$

$$\partial_t\theta = \frac{\delta\mathscr{H}}{\delta\pi} = \frac{\hbar(\nabla\theta)^2}{2m} - \frac{\hbar}{2m\sqrt{\rho}}\nabla^2\sqrt{\rho} + \frac{g}{\hbar}\rho. \tag{9}$$

This system, of course, is fully equivalent to Eq.1 (with $U = 0$) and can be obtained from it directly using the substitution 4. However, it has a very important advantage as pure energy relaxation can be directly introduced to it, as it is discussed below.

Let us first note that Eq. 8 is nothing but a continuity equation for the conserving quantity $\rho$ with current density

$$\mathbf{j} = -\frac{\hbar\rho}{m}\nabla\theta. \tag{10}$$

Pure energy relaxation should not affect particle number conservation, so we can do nothing but leave this equation as is.

On the other hand, energy relaxation can be introduced in Eq. 9 via additional term proportional to $-\delta\mathscr{H}/\delta\theta$, which drags the system towards the state of the minimal energy, so that the modified dynamic equations read:

$$\hbar\partial_t\rho = -\frac{\delta\mathscr{H}}{\delta\theta} = \frac{\hbar^2}{m}\nabla(\rho\nabla\theta), \tag{11}$$

$$\partial_t\theta = \frac{\delta\mathscr{H}}{\delta\pi} - \gamma\frac{\delta\mathscr{H}}{\delta\theta} = \tag{12}$$

$$= \frac{\hbar(\nabla\theta)^2}{2m} - \frac{\hbar}{2m\sqrt{\rho}}\nabla^2\sqrt{\rho} + \frac{g}{\hbar}\rho + \lambda\nabla(\rho\nabla\theta),$$

where $\lambda = \hbar^2\gamma/m$ is a phenomenological energy damping constant. The energy of the system is not any more

constant but decreases with time as

$$\frac{dE}{dt} = \int \frac{\partial \mathscr{H}}{\partial t} d^2\mathbf{r} = -\frac{\lambda\hbar^2}{m} \int \left[\nabla(\rho\nabla\theta)\right]^2 d^2\mathbf{r} = -\lambda m \int |\nabla\mathbf{j}|^2 d^2\mathbf{r} \leq 0. \tag{13}$$

The system thus relaxes to the minimal energy state, conserving the total number of particles.

Note that we can rewrite the equations 11,12 back to a single equation for the field function 4 as follows:

$$i\hbar\frac{\partial\psi}{\partial t} = -\frac{\hbar^2}{2m}\nabla^2\psi + g|\psi|^2\psi - m\lambda\psi\nabla\mathbf{j} = -\frac{\hbar^2}{2m}\nabla^2\psi + g|\psi|^2\psi + \frac{i\hbar}{2}\lambda\psi\left[\psi^*\nabla^2\psi - \psi\nabla^2\psi^*\right]. \tag{14}$$

This equation constitutes the main result of the current work. In the following, we show that the energy relaxation crucially affects both the dispersion of elementary excitations and the spatio-temporal dynamics of polariton droplets.

*Dispersion of elementary excitations and superfluidity.* It is a known fact that the dispersion of elementary excitations of a conservative spatially homogeneous condensate with density $\rho_0$ is gapless and linear in $\mathbf{k}$, and at small momenta is described by the widely known Bogoliubov formula $\omega(k) = \sqrt{g\rho_0/m}\,k$, which according to the Landau criterium corresponds to the onset of superfluidity in the system, with

$$v_c = \sqrt{\frac{g\rho_0}{m}} \tag{15}$$

being a critical velocity.

This result can be obtained directly from Eq. 1 by calculating the dispersion of small excitation on the background of the spatially uniform condensate. We can apply a similar procedure to analyze how the pure energy relaxation will affect the dispersion.

The total field corresponding to a condensate of a density $\rho_0$ and an excitation with wavevector $\mathbf{q}$ and frequency $\omega$ is:

$$\psi(\mathbf{r},t) = e^{-i\frac{g\rho_0}{\hbar}t}\left[\sqrt{\rho_0} + \xi e^{i(\mathbf{q}\cdot\mathbf{r}-\omega t)} + \bar{\xi}^* e^{-i(\mathbf{q}\cdot\mathbf{r}-\omega t)}\right], \tag{16}$$

where $\xi$, and $\bar{\xi}$ are the amplitudes of the small perturbations, $|\xi|^2, |\bar{\xi}|^2 \ll \rho_0$. Placing ansatz Eq.16 in Eq.14 and linearizing it, one gets the following for the dispersion of elementary excitation:

$$\omega(q) = \sqrt{\frac{g\rho_0}{m}q^2 + \left(\frac{\hbar^2}{4m^2} - \frac{\lambda^2\rho_0^2}{4}\right)q^4} - i\frac{\lambda\rho_0 q^2}{2}, \quad (17)$$

The real and imaginary parts of the dispersions are shown in Figure 1. Note that in small $q$ the real part of the dispersion remains linear $\partial\omega/\partial q|_{q=0} = v_c$ and therefore, according to the Landau criterion, the condensate is superfluid with critical velocity $v_c$ independently of $\lambda$. The negative imaginary part is responsible for the decay of the excitations provided by the pure energy relaxation term, which scales quadratically with $q$ and is proportional to the condensate density $\rho_0$, which, as expected, reflects the effect of bosonic stimulation.

Let us remark that both the effect of polariton superfluidity [7, 8] and the formation of a linear polariton dispersion above the condensation threshold in a dissipative system was reported experimentally [15, 16]. Note also that models of dissipative polariton fluids without pure energy relaxation give a qualitatively different dispersion, with flat regions in energy bands [11, 17], and no clean superfluid behavior [18].

The onset of a superfluid behavior in our model can be directly tested numerically. Consider an obstacle moving across a uniform condensate corresponding to a field function $\psi = \sqrt{\rho_0}$ and described by the external potential in the form of a Gaussian function $V = V_0\exp\left[-(x - v_p t)^2/w_p^2\right]$ where $V_0$, $w_p$ and $v_p$ are the depth, width and velocity of the potential.

The results of the 2D simulations are shown in Fig. 2. The four upper panels illustrate the supersonic cases of obstacle motion in the absence (a),(b) and in the presence $\lambda = 1.4 \cdot 10^{-3}$ $\mu m^4 \cdot ps^{-1}$ of the energy relaxation. The cones of the emitted waves are clearly seen in panels (a),(c). In the corresponding spatial spectra, see panels (b), (d), there are characteristic patterns corresponding to the phase matching condition $\text{Re}[\omega(\mathbf{q})] = v_p q_x$, where $\mathbf{q}$ is a wavevector of a scattered wave. The difference introduced by the energy relaxation is that in this case the emitted waves slowly decay so that the field becomes localized (c), and the amplitudes of the scattered waves with high momenta are suppressed (compare panels (b) and (d)), since the decay rate of the linear excitations
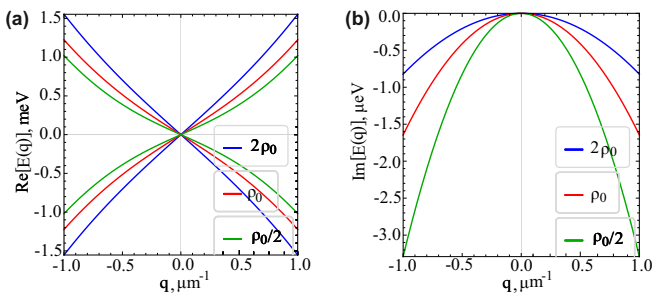
FIG. 1. The real (a) and imaginary (b) parts of the dispersion $E(q) = \hbar\omega(q)$ for different condensate densities $\rho_0$. The condensate is resting in the laboratory reference system (the phase gradient of $\psi$ is equal to zero). The real part of dispersion shows linear scaling with $q$ at small momenta, characteristic of superfluid behavior. The critical superfluid velocity increases with the density, as expected. The imaginary part of dispersion is responsible for the decay of the excitations provided by the pure energy relaxation term and scales quadratically with $q$. Parameters of the system are $g = 6 \cdot 10^{-3}\ meV \cdot \mu m^2$, $m = 5 \cdot 10^{-5}m_0$, $\rho_0 = 100\ \mu m^{-2}$, $\lambda = 0.5 \cdot 10^{-4}\mu m^4 \cdot ps^{-1}$.

with $\mathbf{q}$ is proportional to $\mathrm{Im}[\omega(\mathbf{q})] \sim \mathbf{q^2}$. In the case of the subsonic regime, no emitted waves have been observed, and this regime is very similar to that known for unperturbed GPE (see panels (e) and (f)).

*Stability of superfluid and non-superfluid flows.*

All stationary solutions of GPE are also solutions of (14). This follows from the fact that for that solution $\nabla \mathbf{j} = \mathbf{0}$ and the term accounting for the relaxation vanishes. However, relaxation does affect the stability of solutions. To analyze this, one should use Eq. 14 the ansatz corresponding to a spatially uniform condensate propagates along the $x$ axis with the wavevector of the absolute value $\kappa$,

$$\psi(\mathbf{r}, t) = e^{-i(\frac{g\rho_0}{\hbar} + \frac{\hbar\kappa^2}{2m})t + i\kappa x}\left[\sqrt{\rho_0} + \xi e^{i(\mathbf{q}\cdot\mathbf{r}-\omega t)} + \bar{\xi}^* e^{-i(\mathbf{q}\cdot\mathbf{r}-\omega t)}\right] \tag{18}$$

and then perform the linearization procedure. This gives the following dispersion relation for the excitations:

$$\omega(q) = \sqrt{\frac{g\rho_0}{m}q^2 + \left(\frac{\hbar^2}{4m^2} - \frac{\lambda^2\rho_0^2}{4}\right)q^4 - \frac{i\hbar q^2}{m}\lambda\rho_0\kappa q_x} - i\frac{\lambda\rho_0 q^2}{2} + \frac{\hbar}{m}\kappa q_x, \tag{19}$$

Note that for $\kappa = 0$ Eqs.17 and 19 are equivalent. However, differently from Eq.17 the imaginary part of Eq.19 can become positive, resulting in the development of the flow instability. The typical dependence of the instability increment (positive imaginary part of (17)) for an unstable condensate is shown in Fig. 3(a) as a function of $q_x$, $q_y$.

The dependency of the maximum instability increment as a function of $\rho_0$ and $\kappa$ is shown in Fig. 3(b). As expected, it is higher for fast-moving condensates. However, the dependency on the condensate density $\rho_0$ at fixed $\kappa$ is not monotonous: it is always zero for $\rho_0 = 0$, then grows, reaches its maximum, and then at some density is rolled to zero so that the condensate stabilizes. It happens exactly at the point where the velocity of the condensate becomes equal to the critical velocity defined by the Landau criterion. More details on the development of the instability are given in Supp. Mat.

*Deceleration of polariton droplets.* Let us now analyze how energy relaxation affects the dynamics of polariton droplets. To keep the presentation short, we consider the simplest case of one-dimensional Gaussian wavepacket $\psi(t = 0, x) = \sqrt{\rho_m}\exp(-x^2/w_0^2 + ik_0 x)$ with the maximum density $\rho_m$ and wavevector $k_0$.

We have performed a series of numerical simulations that reveal that the non-zero relaxation energy rate $\lambda \neq 0$ results in the deceleration of the condensate pulse. The dependencies of the velocities of the condensates are defined as $v = d\langle x\rangle/dt$ with $\langle x\rangle = N^{-1}\int x|\psi|^2 dx$, $N = \int |\psi|^2 dx$ are shown in Fig. 4 for different initial peak densities and velocities.

As expected, the deceleration rate increases with the condensate densities; see Supp. Mat. We have checked that at short propagation times the velocity decreased exponentially, $v = v_0\exp(-\gamma t)$ with the decay rate $\gamma$ being independent on $k_0$ and scaling linearly with $\rho_m$. At longer propagation distances the pulse broadens, its intensity decreases, and the velocity scaling with time be-
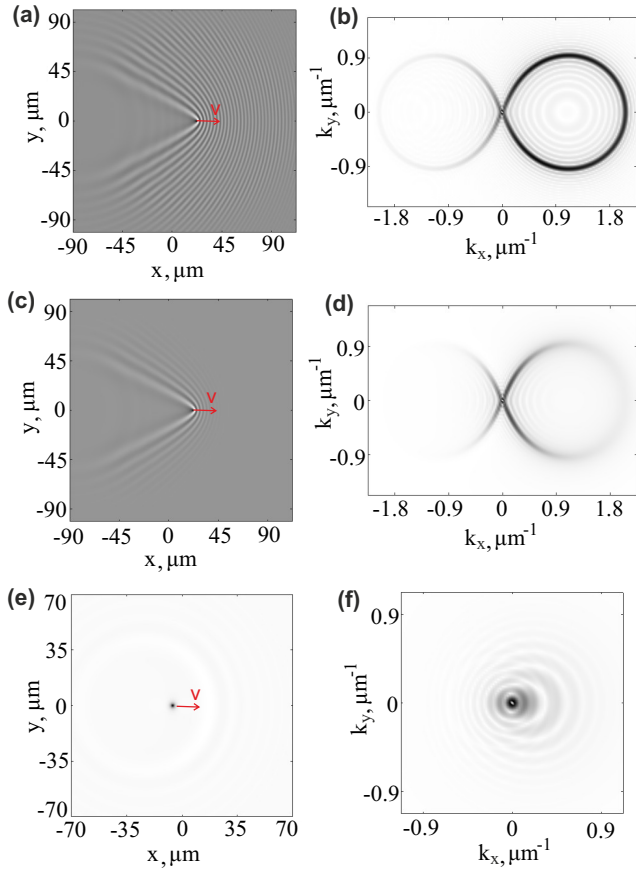
FIG. 2. The density (a) and the spatial spectrum (b) of a supersonic condensate in the presence of an obstacle moving across it, with perturbation potential being $V = V_0 \exp\left[-(x - v_p t)^2 / w_p^2\right]$. The density of the condensate is $\rho_0 = 50\ \mu m^{-2}$, $V_0 = 0.3\ meV$, $w_p = 0.56\ \mu m$, $v_p = 2.5\ \mu m \cdot ps^{-1}$. The nonlinear polariton-polariton interaction $g = 6 \cdot 10^{-3}\ meV \cdot \mu m^2$, the relaxation rate $\lambda = 0$. Panels (c) and (d) show the same but in the presence of the relaxation $\lambda = 1.4 \cdot 10^{-3} \mu m^4 \cdot ps^{-1}$. Panels (e) and (f) show the same as (c) and (d), but for the subsonic case with $v_p = 0.5\ \mu m \cdot ps^{-1}$.



FIG. 3. Panel (a): increment rate of the perturbations characterized by the wavevectors $q_x$ and $q_y$ (imaginary part of $\omega(\vec{q})$ given by (17)). The density of the condensate is $\rho_0 = 150\ \mu m^{-2}$, the condensate propagates along the $x$ axis with the wavevector $\kappa = 1.3\ \mu m^{-1}$. The parameters are $g = 6 \cdot 10^{-3}\ meV \cdot \mu m^2$, $\lambda = 1.4 \cdot 10^{-3} \mu m^4 \cdot ps^{-1}$. The white lines show the boundary where the increments roll to zero. Panel (b): maximum increment of the instability as a function of the condensate density $\rho_0$ and its wavevector $\kappa$. The white line shows the border separating the stable condensate (above the curve) and unstable condensate (below the curve). At $\rho = 0$ the condensate is neutrally stable.



FIG. 4. Panel (a): dependencies of the condensate droplet velocity $v$ on the propagation time $t$ for initial wavevector $k_0 = 0.7\ \mu m^{-1}$ and different initial peak densities $\rho_m = 50\ \mu m^{-2}$ (black curve), $\rho_m = 125\ \mu m^{-2}$ (blue curve) and $\rho_m = 200\ \mu m^{-2}$ (red curve). Panel (b) shows the same, but for the initial wavevector $k_0 = 2\ \mu m^{-1}$. For all cases $g = 0$ and $\lambda = 1.4 \cdot 10^{-3} \mu m^4 \cdot ps^{-1}$.

comes polynomial, $v \sim t^{-2}$. Polartion-polariton interactions are repelling, so that they speed up the condensate spreading and thus suppress its deceleration. A detailed discussion of these effects will be presented elsewhere.

*Conclusion* We have shown that the pure energy relaxation can be naturally introduced into the Gross-Pitaevskii equation. The resulting dissipation term conserves the number of particles and does not destroy the effect of superfluidity but strongly affects the dynamics of polariton droplets. Our results can also be applied to the cases of other bosonic condensates where the effects of energy relaxation are important.
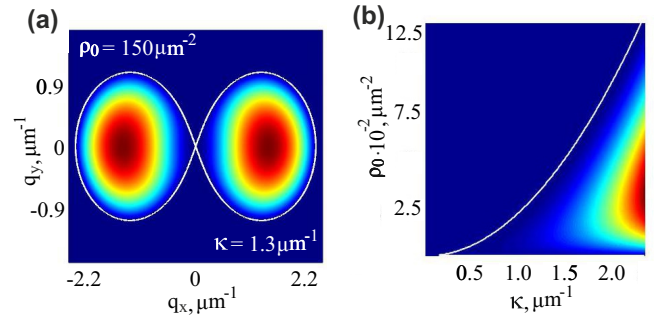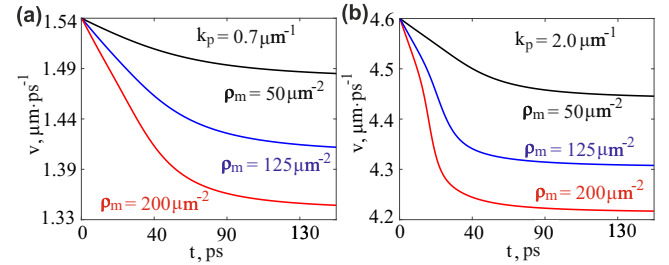
[1] S. Pitaevskii, L.and Stringari, *Bose Einstein Condensation* (Oxford University Press, 2003).

[2] A. V. Kavokin, J. J. Baumberg, G. Malpuech, and F. P. Laussy, *Microcavities* (Oxford University Press, 2017).

[3] I. Carusotto and C. Ciuti, Quantum fluids of light, Rev. Mod. Phys. **85**, 299 (2013).

[4] D. Ballarini, D. Caputo, C. S. Muñoz, M. De Giorgi, L. Dominici, M. H. Szymańska, K. West, L. N. Pfeiffer, G. Gigli, F. P. Laussy, and D. Sanvitto, Macroscopic two-dimensional polariton condensates, Phys. Rev. Lett. **118**, 215301 (2017).

[5] J. Kasprzak, M. Richard, S. Kundermann, A. Baas, J. M. J. Jeambrun, P. Keeling, F. M. Marchetti, M. H.

Szymanska, R. Andre, J. M. Staehli, V. Savona, P. B. Littlewood, B. Deveaud, and L. Si Dang, Bose–einstein condensation of exciton polaritons, Nature **443**, 409 (2006).

[6] R. Balili, V. Hartwell, D. Snoke, and K. West, Bose-einstein condensation of microcavity polaritons in a trap, Science **316**, 1007 (2007).

[7] A. Amo, J. Lefrére, S. Pigeon, C. Adrados, C. Ciuti, I. Carusotto, R. Houdré, E. Giacobino, and A. Bramati, Superfluidity of polaritons in semiconductor microcavities, Nature Phys. **5**, 805 (2009).

[8] G. Lerario, A. Fieramosca, F. Barachati, D. Ballarini, K. S. Daskalakis, L. Dominici, M. De Giorgi, S. A. Maier, G. Gigli, S. Kéna-Cohen, and D. Sanvitto, Room-temperature superfluidity in a polariton condensate, Nature Phys. **13**, 837 (2017).

[9] C. Schneider, A. Rahimi-Iman, N. Y. Kim, J. Fischer, I. G. Savenko, M. Amthor, M. Lermer, A. Wolf, L. Worschech, V. D. Kulakovskii, I. A. Shelykh, M. Kamp, S. Reitzenstein, A. Forchel, Y. Yamamoto, and S. Hofling, An electrically pumped polariton laser, Nature **497**, 348 (2013).

[10] I. Carusotto and C. Ciuti, Probing microcavity polariton superfluidity through resonant rayleigh scattering, Phys. Rev. Lett. **93**, 166401 (2004).

[11] M. Wouters and I. Carusotto, Excitations in a nonequilibrium bose-einstein condensate of exciton polaritons, Phys. Rev. Lett. **99**, 140402 (2007).

[12] M. O. Borgh, J. Keeling, and N. G. Berloff, Spatial pattern formation and polarization dynamics of a nonequilibrium spinor polariton condensate, Phys. Rev. B **81**, 235302 (2010).

[13] L. Pitaevskii, Spontaneous polarization buildup in a room-temperature polariton laser, Sov. Phys. JETP **35**, 282 (1959).

[14] D. D. Solnyshkov, H. Terças, K. Dini, and G. Malpuech, Hybrid boltzmann–gross-pitaevskii theory of bose-einstein condensation and superfluidity in open driven-dissipative systems, Phys. Rev. A **89**, 033626 (2014).

[15] M. Pieczarka, M. Syperek, L. Dusanowski, J. Misiewicz, F. Langer, A. Forchel, M. Kamp, C. Schneider, S. Höfling, A. Kavokin, and G. Skek, Ghost branch photoluminescence from a polariton fluid under nonresonant excitation, Phys. Rev. Lett. **115**, 186401 (2015).

[16] F. Claude, M. J. Jacquet, I. Carusotto, Q. Glorieux, E. Giacobino, and A. Bramati, Spectrum of collective excitations of a quantum fluid of polaritons, Phys. Rev. B **107**, 174507 (2023).

[17] D. D. Solnyshkov, I. A. Shelykh, N. A. Gippius, A. V. Kavokin, and G. Malpuech, Dispersion of interacting spinor cavity polaritons out of thermal equilibrium, Phys. Rev. B **77**, 045314 (2008).

[18] I. Amelio and I. Carusotto, Perspectives in superfluidity in resonantly driven polariton fluids, Phys. Rev. B **101**, 064505 (2020).

D. A. Saltykova,[1] A. V. Yulin,[1] and I. A. Shelykh[2]

[1]*ITMO University, St. Petersburg 197101, Russia*
[2]*Science Institute, University of Iceland, Dunhagi 3, IS-107 Reykjavik, Iceland*
(Dated: April 10, 2025)

*Resonant condition for the waves emitted in the supersonic regime*

The dispersion (17) in the main text can be verified by comparison with the results of direct numerical simulations. We perform numerical simulations of the one-dimensional version of (14) perturbed by a moving potential

$$V = V_0 exp(-\frac{(x - v_p t)^2}{w_p^2}), \qquad (1)$$

where $V_0 = 0.3\ meV$, $w_p = 0.56\ \mu m$. The initial conditions are taken in the form of a resting spatially uniform condensate of the density $\rho_0 = 50\ \mu m^{-2}$.

We observe that the potential produces a radiation tail if the velocity is high enough; in the spectral domain, this effect leads to the appearance of a narrow resonant line. The position $k_r$ of this spectral line can be found from the dispersion characteristics by solving the phase-matching condition

$$Re[\omega(k_r)] = v_p k_r. \qquad (2)$$

So, the resonant wavevector is a function of velocity $k_r(v_p)$. This dependency is shown in Fig. 1(a) by the solid curve. The positions of the resonant spectral lines observed in the numerical simulations of (14) are shown by the blue circles in the same plot. One can see that all dots are situated on the analytical curve, and so we can claim that the numerical simulations are in very good agreement with the numerics.

To check the imaginary part of the dispersion characteristic, we can extract the decay rate of the resonantly emitted waves in the numerical simulations of (14). We observe that in the stationary regime, the wave resonantly emitted by the moving obstacle decays exponentially in space, with a certain propagation length $L_d$ depending on the velocity of the obstacle. The relative velocity of the radiation with respect to the potential is $|v_g - v_p|$, where $v_g = Re[\partial_k \omega|_{k_r}]$ is the group velocity of the emitted waves. Thus, the spatial decay rate $\frac{1}{L_d}$ is related to the decay rate in time as

$$\frac{1}{L_d} = Im[\omega(k_r)] \frac{1}{|v_g - v_p|}. \qquad (3)$$

So, the imaginary part of the dispersion can be extracted from the results of the numerical simulations using the
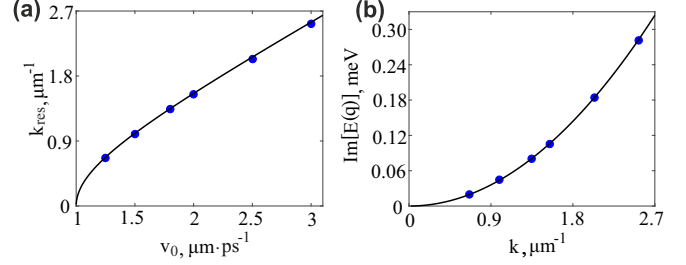


FIG. 1. Panel (a) shows the dependence of the resonant wavevector of the emitted waves on the velocity of the moving localized potential obtained from the phase matching condition. The blue circles show the positions of the resonant spectral lines in the spatial spectrum of the condensate field obtained by direct numerical simulations of Eq.(14) in the main text. Panel (b) shows the dependency of the imaginary part of the dispersion characteristic (solid line) and the decay rate of the resonant radiation extracted from the numerical simulations. The simulations and analytics are done for the spatially uniform condensate of density $\rho_0 = 50\ \mu m^{-2}$, the polariton-polariton interaction $g = 6 \cdot 10^{-3} meV \cdot \mu m^2$, the energy relaxation $\lambda = 1.4 \cdot 10^{-3} \mu m^4 \cdot ps^{-1}$, the potential is given by $V = V_0 exp(-\frac{(x - v_p t)^2}{w_p^2})$ with the depth $V_0 = 0.3\ meV$ and width $w_p = 0.56\ \mu m$.

formula

$$Im[\omega(k_r)] = \frac{|v_g - v_p|}{L_d}. \qquad (4)$$

The imaginary parts of the eigenfrequencies found by formula (14) are shown in panel (b) of Fig. 1 by the solid line. The blue circles show the eigenfrequencies extracted from the numerical simulations. It can be seen that the decay rate found in the numerical simulations also agrees well with its analytical counterpart.

*The development of the instability*

Let us discuss the stability of the condensate moving in the reference frame at a velocity higher than the critical velocity. As long as the velocity in the laboratory reference frame is less than the critical velocity of the condensate, the condensate is stable, according to formula (19) in the main text. This analytical result perfectly matches our numerical simulations of (14) in the main text with initial conditions taken in the form of a spatially uniform condensate perturbed by weak noise. All excitations decay in time, and the stationary state is the condensate
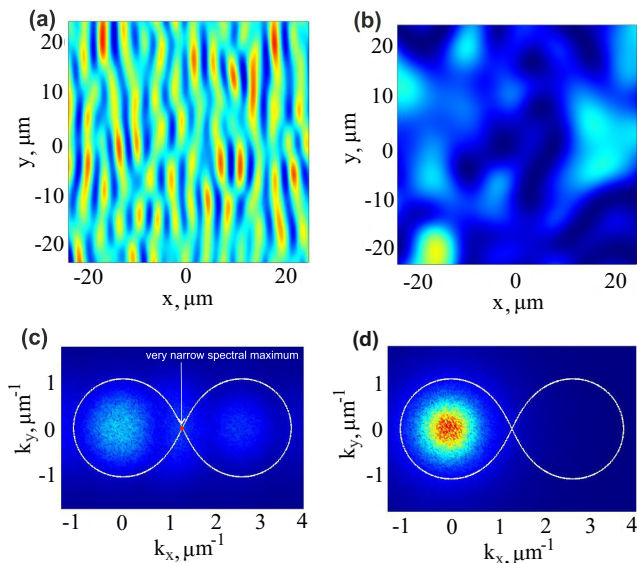
FIG. 2. The deviation of the condensate density from its mean value at $t = 25\ ps$ and $t = 65\ ps$. The initial conditions are taken in the form of a weak noise ovelapped with the spatially uniform condensate with the wavevector of the value $\kappa = 1.3\ \mu m^{-1}$ oriented along the $x$ axis. Panels (c) and (d) show the spatial spectra of the whole field for $t = 25\ ps$ and $t = 65\ ps$ correspondingly. The white curves in panels (c) and (d) indicate the border of the instability range (inside the curve) calculated by formula (19) in the main text. The other parameters are $g = 6 \cdot 10^{-3} meV \cdot \mu m^2$ and $\lambda = 1.4 \cdot 10^{-3} \mu m^4 \cdot ps^{-1}$.

moving at the same velocity as in the beginning (up to the precision of our numerical simulations).

We also observed that, in full accordance with formula (19) in the main text, the condensate moving at supersonic velocity is unstable and perturbations start growing. This process is illustrated in Fig. 2(a),(b) showing the deviation of the condensate density from its average value for the intermediate time (quasi-linear stage of the instability) and at a relatively long time when the instability is practically saturated.

It can be noticed that vertically oriented stripes appear at first. The period of the stripe is defined by the wavevector at which the instability growth rate given by (19) reaches its maximum. Panel (c) of the figure shows the spectrum of the field. This spectrum has a very narrow maximum located at $k_x = 1.3\ \mu m^{-1}$, $k_y = 0$, which corresponds to the initial state of the condensate. The white curve shows the border of the instability in $k$ space. It is clear that there is indeed an increase in spectral harmonics inside the curve.

The developed stage of the instability is shown in panel (b). There are some large-scale variations of the condensate density, but no developed quasiperiodic stripes are seen anymore. The spectrum of the field is shown in (d). The spectrum is nearly completely local-
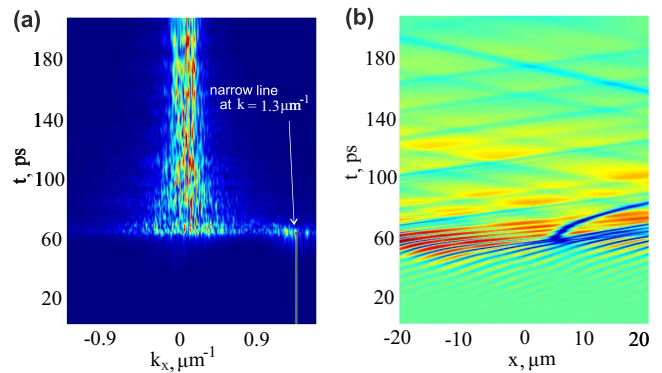


FIG. 3. The temporal development of the one-dimensional condensate with $\kappa = 1.3\ \mu m^{-1}$. The initial conditions are the spatially uniform condensate of density $\rho_0 = 50\ \mu m^{-2}$ perturbed by weak noise. Panel (a) shows evolution of the spectrum and panel (b) shows evolution of the field. The other parameters are $g = 6 \cdot 10^{-3} meV \cdot \mu m^2$, $\lambda = 1.4 \cdot 10^{-3} \mu m^4 \cdot ps^{-1}$.

ized near $k = 0$. Thus, we can say that the development of the instability is the mechanism leading to the deceleration of the condensate.

The development of the instability in the one-dimensional condensate is shown in Fig. 3. It is seen that at time $t \approx 65\ ps$ the quasiperiodic excitations develop. In the spectral representation, it corresponds to the formation of the second maximum, which is less intense and much wider than the first one. Finally, the initial spectral line disappears and only harmonics with small $k$ survive. Let us remark that for $g = 0$ the short-scale excitations disappear much faster than for relatively large $g$. This can be an indication that some of the short-scale excitations are, actually, dark solitons (1D analogue of vortices) forming in the condensate.

*The evolution of the field and the spectrum of the condensate droplets*

The evolutions of the field and the spectrum of propagating condensate droplets are shown in panels (a) and (b) of Fig. 4 respectively. The shape of the condensate droplet is seen to change during propagation. First, it gets wider, and second, it becomes asymmetric. Both the spreading rate and the rate of asymmetry development increase with the maximum density of the droplet. In the spectral domain, it is seen that the range of the wavevectors filled by the condensate shifts towards smaller $k$'s during propagation. This means deceleration of the droplet because in these regimes the velocity of the droplet is very accurately approximated by the group velocity of linear waves calculated at the central wavevector.

To show how the density of the condensate affects the mean value of the wavevector and the width of the spatial spectrum of the condensate, we calculate the dependen-
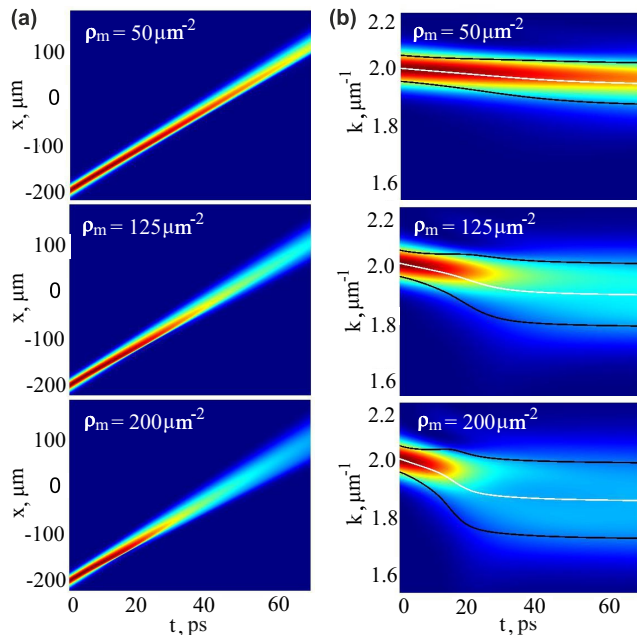
FIG. 4. Panel (a) shows the temporal evolution of the propagating droplet. At $t = 0$ the field envelope is Gaussian $\psi(x, t=0) = \sqrt{\rho_m}\exp(-\frac{x^2}{w_p^2})\exp(ik_0 x)$, where $\rho_m$ is the initial maximum of the condensate density, $w_p = 19.1\ \mu m$ is the width of the droplet, and $k_0 = 2\ \mu m^{-1}$ is its initial central wavevector. The upper picture of the panel corresponds to $\rho_m = 50\ \mu m^{-2}$, the middle to $\rho_m = 125\ \mu m^{-2}$ and the bottom one to $\rho_m = 200\ \mu m^{-2}$. The evolution of the spatial spectra of the droplets is shown in panel (b). The white line marks the central wavevector defined as $k_c = \int k S(k)dk/N$, the black lines are $k_c \pm \Delta_{k\,S}$, where $\Delta_{k\,S} = \sqrt{\int (k-k_c)^2 S(k)dk/N}$. The physical meaning of the black lines is that they show the area filled by the condensate. The other parameters are $g = 0$, $\lambda = 1.4 \cdot 10^{-3}\mu m^4 \cdot ps^{-1}$.



FIG. 5. Numerically calculated dependencies of the mean wavevector $k_c = \int k S(k)dk/N$ and the spectrum width $\Delta_{k\,S} = \sqrt{\int (k-k_c)^2 S(k)dk/N}$ on the maximum density $\rho_m$ of the initial condensate droplet are shown in panels (a) and (b) correspondingly. The parameters of the spatial spectrum of the condensate are measured after propagation time $t = 75\ ps$. The initial condensate field distribution is Gaussian $\psi(x, t=0) = \sqrt{\rho_m}\exp(-\frac{x^2}{w_p^2})\exp(ik_0 x)$ with the width $w_p = 19.8\ \mu m$. The blue line corresponds to the droplets with the initial mean wavevector $k_0 = 0.7\ \mu m^{-1}$, the red curves are for $k_0 = 2\ \mu m^{-1}$. The other parameters are $g = 0$, $\lambda = 1.4 \cdot 10^{-3}\mu m^4 \cdot ps^{-1}$.

cies of these parameters on the maximum density of the initial distribution of the condensate after relatively long propagation time. The results are summarized in Fig. 5. Let us note that for the chosen parameters, the velocity of the condensate is equal to its wavevector with good accuracy. Our conclusion is therefore that energy relaxation, as expected, results in a decrease in the mean wavevector and hence in a decrease in the droplet velocity. This effect also leads to a broadening of the spectrum. For energy relaxation to be a nonlinear effect, the spectrum modification is more pronounced for the droplets with higher maximum densities.

Next, we study the evolution of the velocity of the Gaussian droplets and find that there are asymptotics at short and long times. To do this, we introduce the quantity
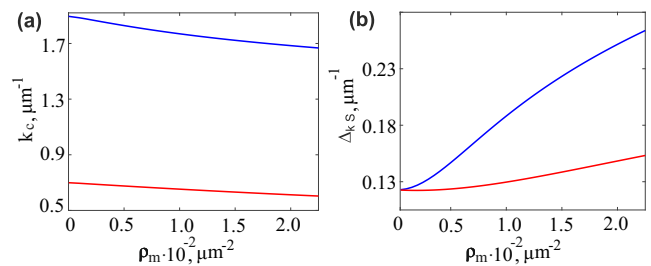
$$z = -\frac{\dot{v}}{v}.$$

The dependencies of these parameters on time are shown in Fig. 6(a),(b) on the double logarithmic scale for different initial wavevectors $k_0$ and maximum densities $\rho_m$ of the condensate. It is seen that in a short time the dependencies look as horizontal straight lines, and so $z$ can be approximated by a constant. This means that $\dot{v} = -\gamma v$ and, consequently,

$$v(t) = v_0 \exp(-\gamma t).$$

Let us note that the equation that governs the evolution of the droplet at short propagation times coincides with the equation for a particle moving under the action of the viscous friction force.

In our equations, the non-linear terms (energy relaxation) scale linearly with the condensate density, and from this we can expect that the deceleration rate $\gamma$ should also be proportional to $\rho_m$. We check that indeed this is the case, and the deceleration rate can be expressed as $\gamma = \gamma_0 \rho_m$. From our numerical simulations, we find that $\gamma_0 \approx 0.17\ \mu m^2 \cdot ps^{-1}$ for the Gaussian pulse of the width $w_p = 19.1\ \mu m$.

The fits overlapped with the numerically calculated dependencies of the droplet velocity on time are shown in Fig. 6(c),(d). It is seen that the fit describes the evolution of the velocity well at short propagation times. At longer times, the dispersive spreading of the envelope starts to play a role, and the fit becomes inapplicable.

More surprisingly, there are asymptotics that work at long propagation times. As one can see in Fig. 6(a),(b) the dependencies $z(t)$ look like inclined straight lines on
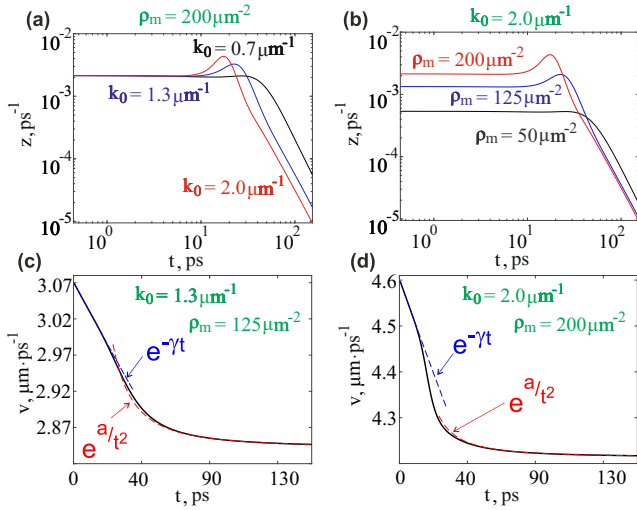
FIG. 6. The numerically calculated dependencies of the parameter $z = -\frac{\dot{v}}{v}$ plotted in double logarithmic scale are shown in panels (a) and (b). In panel (a), the maximum initial density is fixed to $\rho_m = 200 \ \mu m^{-1}$ and the dependencies are plotted for the initial wavevectors of the condensate $k_0 = 2 \ \mu m^{-1}$ (red curve), $k = 1.3 \ \mu m^{-1}$ (blue curve) and $k_0 = 0.7 \ \mu m^{-1}$ (black curve). Panels (b) show the dependencies $z(t)$ for fixed initial $k_0 = 2 \ \mu m^{-1}$ and different maximum densities $\rho_m = 200 \ \mu m^{-2}$ (red curve), $\rho_m = 125 \ \mu m^{-2}$ (blue curve) and $\rho_m = 50 \ \mu m^{-2}$ (black curve). The dependencies of the velocities of the condensate droplets on time are shown in panels (c) and (d) for $k_0 = 1.3 \ \mu m^{-1}$, $\rho_m = 125 \ \mu m^{-1}$ and $k_0 = 2 \ \mu m^{-1}$, $\rho_m = 200 \ \mu m^{-2}$ correspondingly. The fits $v \sim \exp(-\gamma t)$ (blue curves) and $v \sim \exp(\frac{a}{t^2})$ (red curves) working at short and long propagation times are also shown in these panels. The other parameters are $w_p = 19.1 \ \mu m$, $g = 0$, $\lambda = 1.4 \cdot 10^{-3} \mu m^4 \cdot ps^{-1}$.

the double logarithmic scale at large $t$. We checked that

$$z \sim \frac{1}{t^3}$$

at large $t$. So, the velocity can be fitted by

$$v = \tilde{v} \exp(\frac{a}{t^2})$$

where $\tilde{v}$ is the limiting value of the velocity and $a$ is a constant that can be found from numerical simulations. The velocity decays to $\tilde{v}$ as $v = \tilde{v} + \frac{a\tilde{v}}{t^2}$. Analyzing fits overlapped with the numerically calculated dependencies $v(t)$ (See Fig. 6(c),(d)), we can note that the fit describes the evolution of the velocity quite accurately.